JOURNAL OF Applied Polymer SCIENCE

Thermal, Mechanical, and Rheological Properties of Poly(ε-caprolactone)/Halloysite Nanotube Nanocomposites

Kang-Suk Lee,[1] Young-Wook Chang[1,2]

[1]Department of Bio-Nano Technology, Hanyang University, Ansan, Gyeonggi 426-791, Republic of Korea

[2]Polymer Nano Materials Laboratory, Department of Chemical Engineering, Hanyang University, Ansan, Gyeonggi 426-791, Republic of Korea

Correspondence to: Y.-W. Chang (E-mail: ywchang@hanyang.ac.kr)

ABSTRACT: Naturally available halloysite nanotubes (HNTs) with hollow nanotubular structures were used as reinforcement in poly(ε-caprolactone) (PCL). The PCL/HNT nanocomposites were prepared by melt mixing the polymer with as-received HNTs up to 10 wt % in an internal batch mixer. Transmission electron microscopy analysis indicated that the HNTs were dispersed uniformly on the nanoscale throughout the PCL matrix. Differential scanning calorimeter studies revealed that the PCL crystallinity was decreased in the nanocomposites, and the HNTs dispersed in the PCL matrix led to an increase in the non-isothermal crystallization temperature of the PCL. Tensile and dynamic mechanical tests showed great enhancement in strength and stiffness at low HNT content, while still maintaining the ductility of the PCL. The glass transition temperature (T_g) of the pristine PCL was substantially increased with increase in filler loading, which indicates good reinforcing effect imparted by the addition of HNT. Melt rheological studies revealed that the nanocomposites exhibited strong shear thinning behavior, and a percolated network of HNT particles was formed. © 2012 Wiley Periodicals, Inc. J. Appl. Polym. Sci. 000: 000–000, 2012

KEYWORDS: nanostructured polymers; properties and characterization; structure–property relations

Received 2 April 2012; accepted 9 August 2012; published online

DOI: 10.1002/app.38457

INTRODUCTION

The reinforcement of polymers by the addition of nanofillers such as clay minerals or carbon nanotube (CNT) has attracted considerable attention during recent decades because the nanocomposites exhibit greatly improved physical and mechanical properties or new functional properties at relatively low inorganic filler loading levels as compared to the conventional microcomposites.[1–4] Halloysite nanotube (HNT), a type of naturally occurring clay mineral with a chemical composition similar to kaolin having chemical formula $Al_2Si_2O_5(OH)_4{\cdot}2H_2O$, is attracting interest as a new class of nanofiller to reinforce polymers. HNT features a tubular structure resembling CNTs with a high length-to-diameter ratio (L/D), low hydroxyl group density on the surface, and biocompatibility.[5] Typically, the size of HNT nanoparticles varies from 50 to 70 nm in external diameter and 100–2000 nm in length, with about a 15 nm diameter lumen.[6–8] It is noteworthy to mention that the cost effectiveness, natural availability, and biocompatibility of HNT makes it one of the superior nanofiller than that of CNT and nanoclays. The nanorods-like geometry of HNT is not intertwined with each other like CNT or not interlinked like layered silicates; as a consequence the HNT dispersion in the polymer matrix is easier. The overall material properties of the polymers are enhanced by many folds without hampering its inherent transparency at lower HNT loading. It has been reported that the HNTs confer enhanced mechanical properties, thermal stability, and anti-flammability characteristics to polymer matrices likely polyethylene,[9] polypropylene,[10] nylons,[11–13] epoxy resin,[14] and rubbers.[15–17]

The poly(ε-caprolactone) (PCL) is an important biodegradable and biocompatible aliphatic polyester, which has been widely considered for environmentally friendly packaging, medical applications, and pharmaceutical controlled release systems.[18] Some nanofillers such as layered silicates,[19–23] silica,[24] or CNTs[25,26] have been utilized to improve mechanical properties, barrier properties, and the crystallization rate of PCL, and may promote the wider applications of PCL. The HNT is an effective and cheap nanofiller alternative to CNT due to its similar nanotubular structure that may significantly enhance the overall properties of the PCL matrix.

The main objective of the present work deals with the preparation of HNT-based PCL nanocomposites by melt compounding method. Various characterization techniques were employed to

Applied Polymer SCIENCE

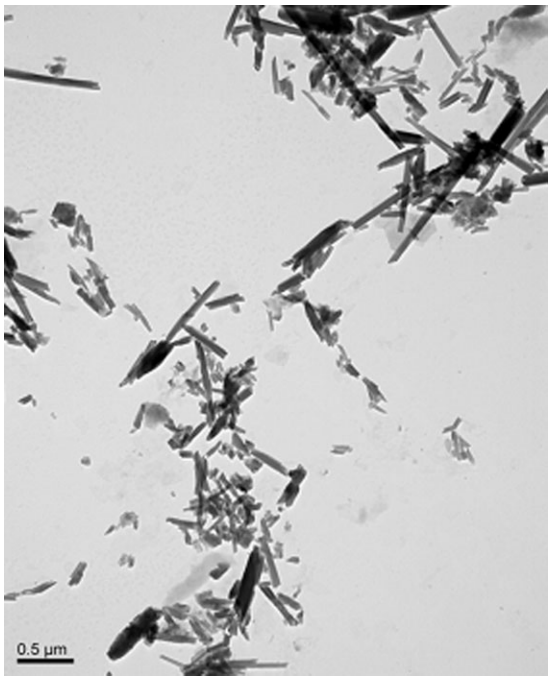

Figure 1. TEM micrograph of HNTs used in this study.

investigate the morphology, thermal, mechanical, and rheological properties of the PCL/HNT nanocomposites. The prepared PCL/HNT nanocomposites may provide vast range of various structural and functional applications likely to fit for consumable products, packaging, biomedical, and many more fields.

EXPERIMENTAL

Materials and Sample Preparation

The tubular HNT shown in Figure 1 was purchased from Sigma-Aldrich Co. LLC., Missouri, USA and was used without any chemical modification. The HNT has specific gravity of 2.53, surface area of 64 m^2/g, pore volume of 1.26–1.34 mL/g, cation exchange capacity of 8.0 meq/g, and zeta potential of −22.543 mV. The HNT particle size distribution analyzed by dynamic light scattering (DLS) measurement is shown in Figure 2. The average hydrodynamic diameter of the HNT is 260 nm in number distribution. The X-ray fluorescence (XRF) spectroscopy analysis revealed that the major composition of the HNT consists of 45.212% Al_2O_3 and 48.797% SiO_2 in the ratio of 1:1.079 along with 5.991% other metal and non-metal oxides as impurities.

The PCL (M_w = 80,000, polydispersity index (PDI) = <2, and density = 1.145 gm/cm^3) was also purchased from Aldrich. PCL/HNT nanocomposites with an HNT content of 3, 5, 7, and 10 wt % were prepared by melt mixing in a Haake Rheocorder at temperature of 100°C using a rotor speed of 60 rpm with a mixing time of 10 min. The compounds obtained were compression molded into 1.0 mm thick sheets at 100°C with an applied pressure of 15 MPa for 10 min.

Measurement and Characterizations

Dynamic Light Scattering. The particle size distribution and zeta potential of the HNT were measured using DLS-800 (Otsuka Electronic, Osaka, Japan) at a fixed scattering angle of 20° in distilled water medium.

X-Ray Fluorescence Spectroscopy. The elemental compositions of HNT were analyzed by means of RIX 3000 (Rigaku Corporation, Tokyo, Japan) XRF spectrometer.

Contact Angle Measurement. The initial water contact angle (WCA) of pristine HNT, neat PCL, and PCL/HNT nanocomposites were determined using a Phoenix 300 contact angle analyzer (SEO Co., Lathes, South Korea) at room temperature.

X-Ray Photoelectron Spectroscopy. X-ray photoelectron spectroscopy (XPS) spectra of neat PCL, PCL/HNT nanocomposites were recorded by using an X-ray photoelectron spectrometer (K-Alpha, Thermo Fisher Scientific, Inc., Massachusetts, USA) with Aluminum (mono) Kα X-ray source (1486.6 eV) operated at 15 kV voltage and 10 mA current. The high-resolution survey was performed for all the samples at spectral regions related to carbon and silicon atoms.

Transmission Electron Microscopy. The dispersibility of the HNT in the composite was examined using transmission electron microscopy (TEM), with a JEOL 200CX TEM with an acceleration voltage of 200 kV. The ultra-thin sections were cut from the compression molded specimens with a thickness of 100 nm using a Reichert ultracut cryo-microtome.

Dynamic Mechanical Analysis. The dynamic mechanical properties of the PCL/HNT nanocomposites were carried out by dynamic mechanical analysis (DMA) (model DMA2980, TA instruments, New Castle, DE). The test temperature range is −100 to +100°C at an applied frequency of 1 Hz and strain amplitude of 10 μm with a scan rate of 2°C/min in liquid nitrogen atmosphere. The tension mode method with samples of dimension 30 × 6.5 × 2 mm^3 were employed to measure the storage modulus (E'), loss modulus (E''), and tan δ parameters. Three specimens were measured for each composition of sample to verify the authenticity of the experimental results. The T_g of the samples was measured from the tan δ peak temperature

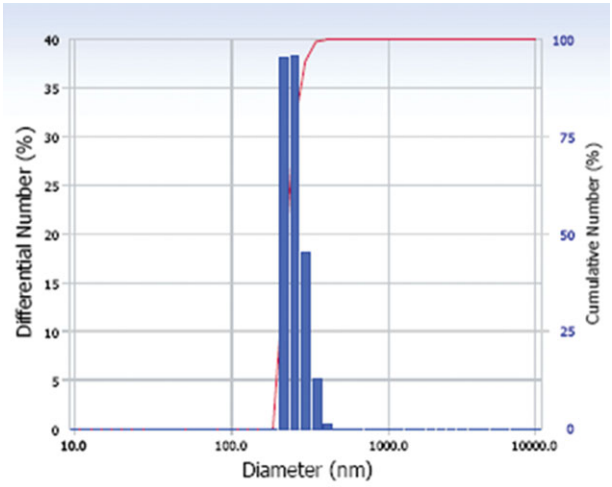

Figure 2. DLS plot of HNT. [Color figure can be viewed in the online issue, which is available at wileyonlinelibrary.com.]

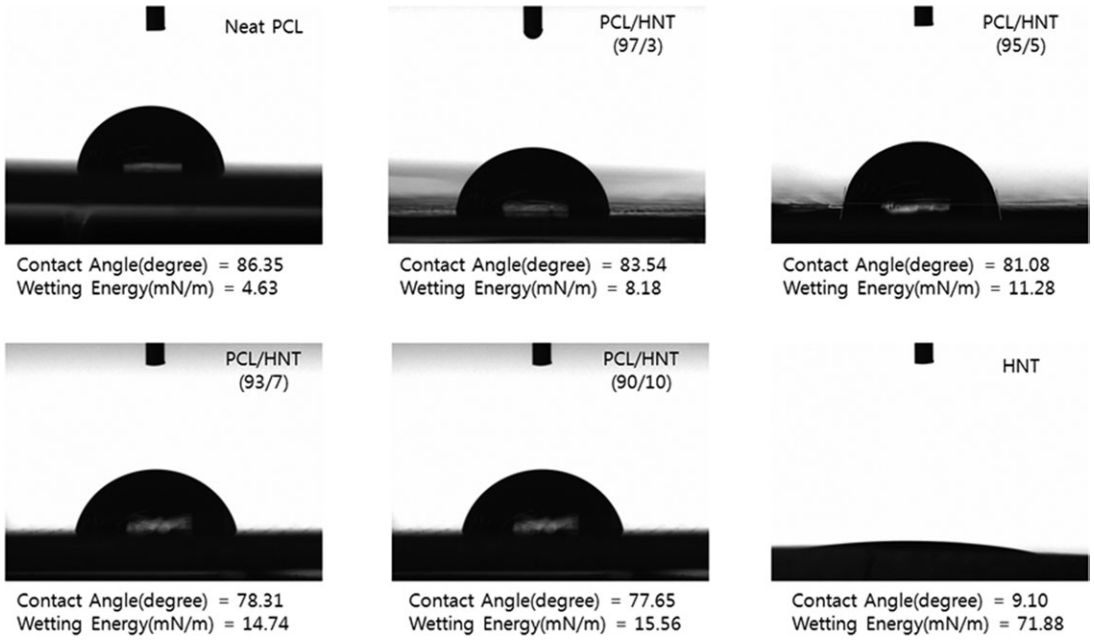

Figure 3. Contact angle measurement of the pristine HNT, neat PCL, PCL/HNT nanocomposites.

because it occurs at the highest temperature and is used historically in literature. It is a good measure of the leather-like midpoint between the glassy and rubbery states of a polymer.[27]

Differential Scanning Calorimetry. The melting temperature (T_m), crystallization temperature (T_c), and heat of fusion (ΔH_m) of the neat PCL and PCL/HNT nanocomposites were determined by using differential scanning calorimeter (DSC 2010, TA Instruments). Samples (10 mg) were dried completely in a vacuum oven prior to DSC analysis. Samples were first heated from 30 to 100°C at a rate of 10°C/min under a nitrogen atmosphere followed by keeping it at 100°C for 10 min to remove the prior thermal history. The samples were then cooled to 0°C at a rate of 10°C/min (first cooling scan) and the crystallization peak temperature (T_c) was determined from the thermogram. Subsequently, the sample was reheated to 80°C at a rate of 10°C/min (second heating scan). The T_m and ΔH_m of the samples were determined from this second scan. Three samples were measured for each composition to examine the ascertainment of the experimental results.

Mechanical Properties. Tensile properties were determined at 25°C using a universal testing machine (United Co., STM-10E) at a crosshead speed of 50 mm/min as per the ASTMD 412 standard specification.[28] At least five dog-bone shaped samples were used. The initial gauge length of the samples was 20 mm. Elastic moduli were derived from the initial linear part of the stress–strain curves (up to about 1% strain).

Scanning Electron Microscopy. The fracture morphology of the neat PCL and PCL/HNT nanocomposites was observed by field-emission scanning electron microscopy (FE-SEM, JEOL JSM-630F) at an accelerating voltage of 15 kV. All the samples were cryo-fractured after immersing them in liquid nitrogen for about 10 min. The fractured surface is scanned to observe the

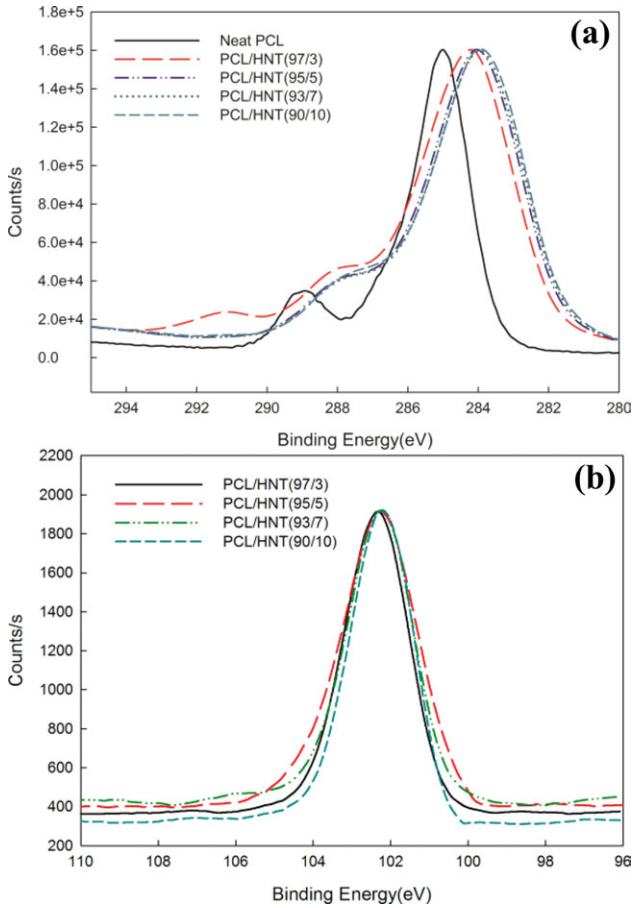

Figure 4. XPS spectra of (a) carbon atom of PCL and (b) silicon atom of HNT. [Color figure can be viewed in the online issue, which is available at wileyonlinelibrary.com.]

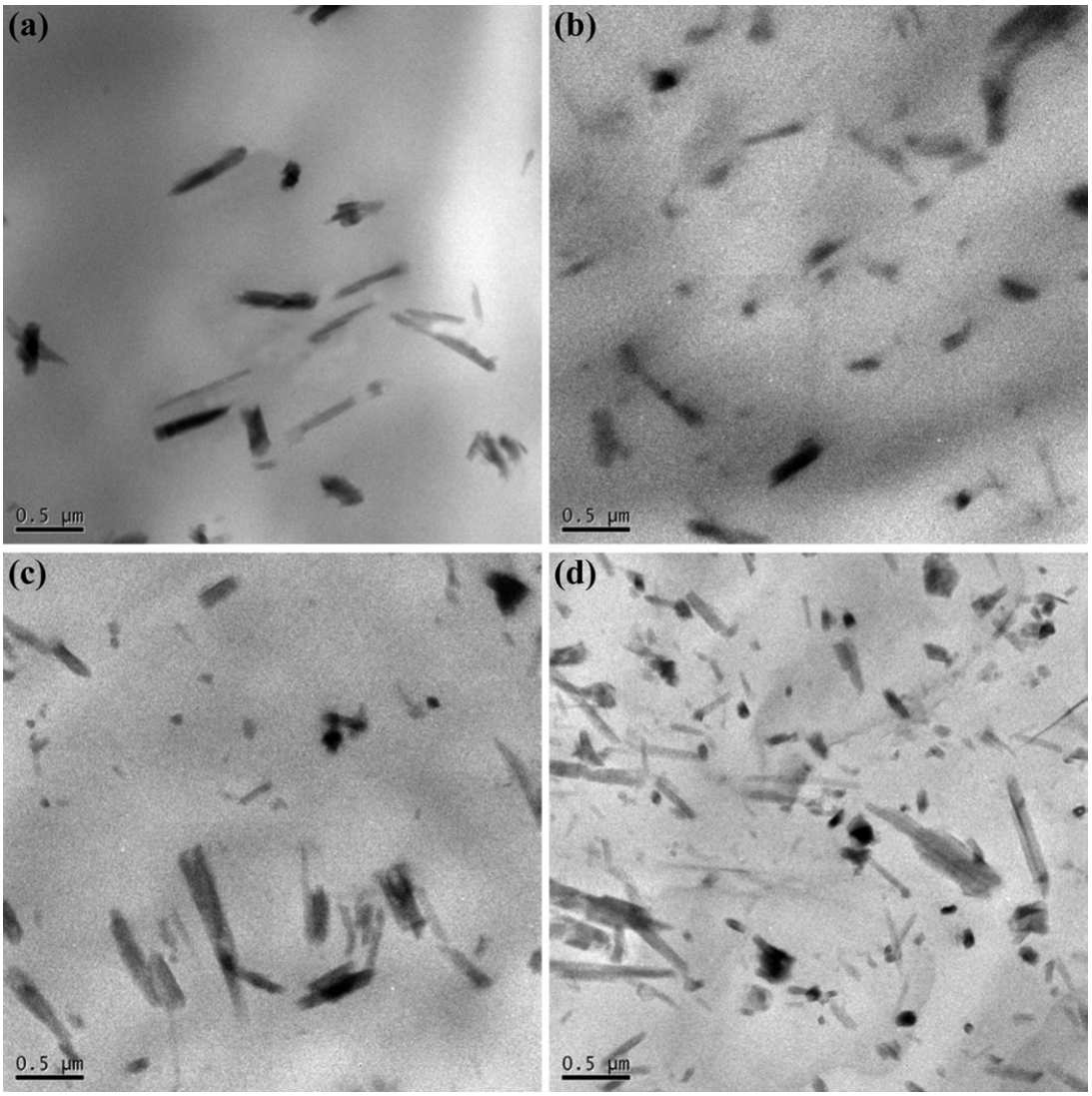

Figure 5. TEM micrographs of PCL/HNT nanocomposites: (a) 97/3, (b) 95/5, (c) 93/7, and (d) 90/10.

dispersion of HNTs. To avoid excessive pull out of the PCL fibrils during fracture, the samples were chilled in liquid nitrogen before breaking to initiate a brittle fracture mechanism. The fracture surface was then coated with a thin layer of gold.

Dynamic Shear Rheology. Melt rheological measurements (small amplitude oscillatory shear rheometry) were carried out in a RDA II Instrument (Rheometrics, Inc., New Jersey, USA). The dynamic oscillatory shear measurements were performed at 100°C using a set of 25 mm diameter parallel plates and a sample 1–2 mm in thickness. The frequency sweep was carried out within the frequency range of 0.1–100 rad/s at a strain of 0.5%, which is well within the linear viscoelastic range. Three samples were tested for each formulation to investigate the validity of the experimental results.

RESULTS AND DISCUSSION

Contact Angle Measurements

The contact angle measurements of pristine HNT, neat PCL, and PCL/HNT nanocomposites were carried out at room temperature with water as solvent medium. Figure 3 shows the pictures of the contact angle measurements. The pristine HNT powder shows contact angle of 9.10°, which indicates that it is strongly hydrophilic in nature, whereas the contact angle of the neat PCL is 86.35° that attributed to the highly hydrophobic characteristic. The hydrophobic nature of the PCL matrix gradually decreases with increase in nanofiller loading due to the increase in wettability of the PCL matrix surface. This reduced tendency of the contact angle confirms the development of noticeable interactions through hydrogen bonding between PCL matrix and HNTs. The wetting energy or surface free energy of the PCL matrix significantly enhanced by the incorporation of the HNT nanotubes, which also concludes that the wetting of liquids is higher in filled systems as compared to the virgin PCL matrix.[29]

X-Ray Photoelectron Spectroscopy

The XPS of samples was carried out to examine the formation of hydrogen bonding between HNT and PCL. The XPS spectra for neat PCL and PCL/HNT nanocomposites are shown in

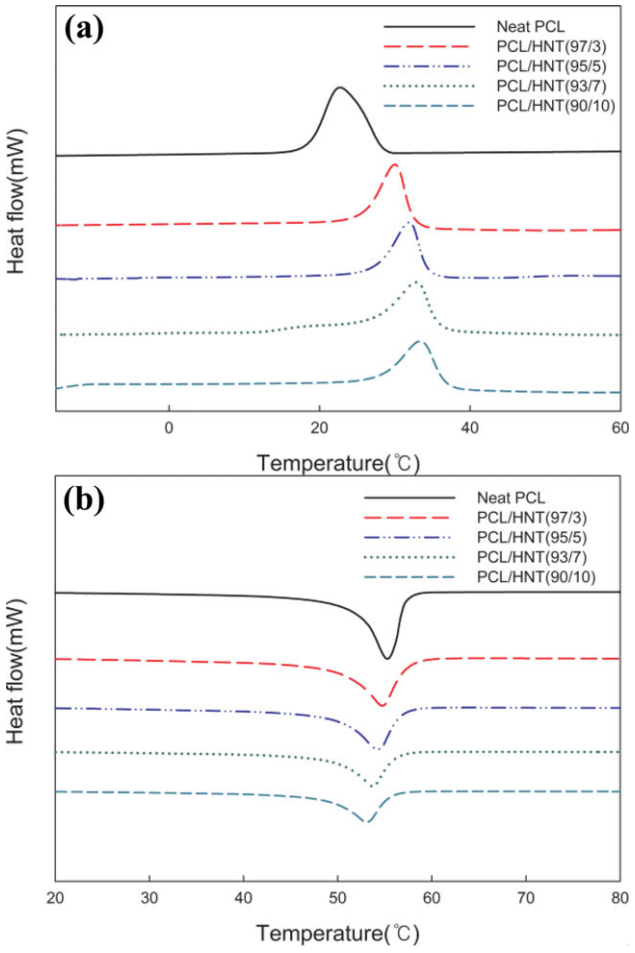

Figure 6. DSC thermograms of neat PCL and PCL/HNT nanocomposites (a) during the cooling process from melt state and (b) during the reheating process. [Color figure can be viewed in the online issue, which is available at wileyonlinelibrary.com.]

Figure 4(a,b). The binding energy is reduced for carbon atom (C^{1s}) from 285.05 to 284.94 eV (0.11 eV) of PCL matrix and from 102.32 to 102.15 eV (0.17 eV) for silicon atom (Si^{2p}) of HNT matrix in case of 10 wt % HNT-filled PCL nanocomposites, which is attributed to the formation of some type of chemical interactions between PCL and HNT. This is due to the formation of strong hydrogen bonding between the hydroxyl group (—OH) present on the HNT surface and carbonyl (—C=O) in ester linkage of the PCL molecular chain.[30]

Table I. Thermal Characteristics of PCL/HNT Nanocomposites

Samples	T_c (°C)	T_m (°C)	ΔH_m (J/g)	χ_c[a] (%)
Neat PCL	22.7 ± 0.02	55.3 ± 0.02	65.0 ± 0.2	48.8
PCL/HNT				
97/3	30.0 ± 0.02	54.8 ± 0.02	60.7 ± 0.2	46.0
95/5	31.9 ± 0.02	54.2 ± 0.02	56.8 ± 0.2	44.0
93/7	32.8 ± 0.02	53.7 ± 0.02	54.7 ± 0.1	43.2
90/10	33.4 ± 0.02	53.1 ± 0.02	51.5 ± 0.1	42.1

[a] $\chi_c = 100 \times (\Delta H_m/\Delta H_m^o)/w$, where ΔH_m^o is the heat of melting for 100% crystalline PCL (136 J/g)[31] and w is the weight fraction of PCL in the nanocomposites.

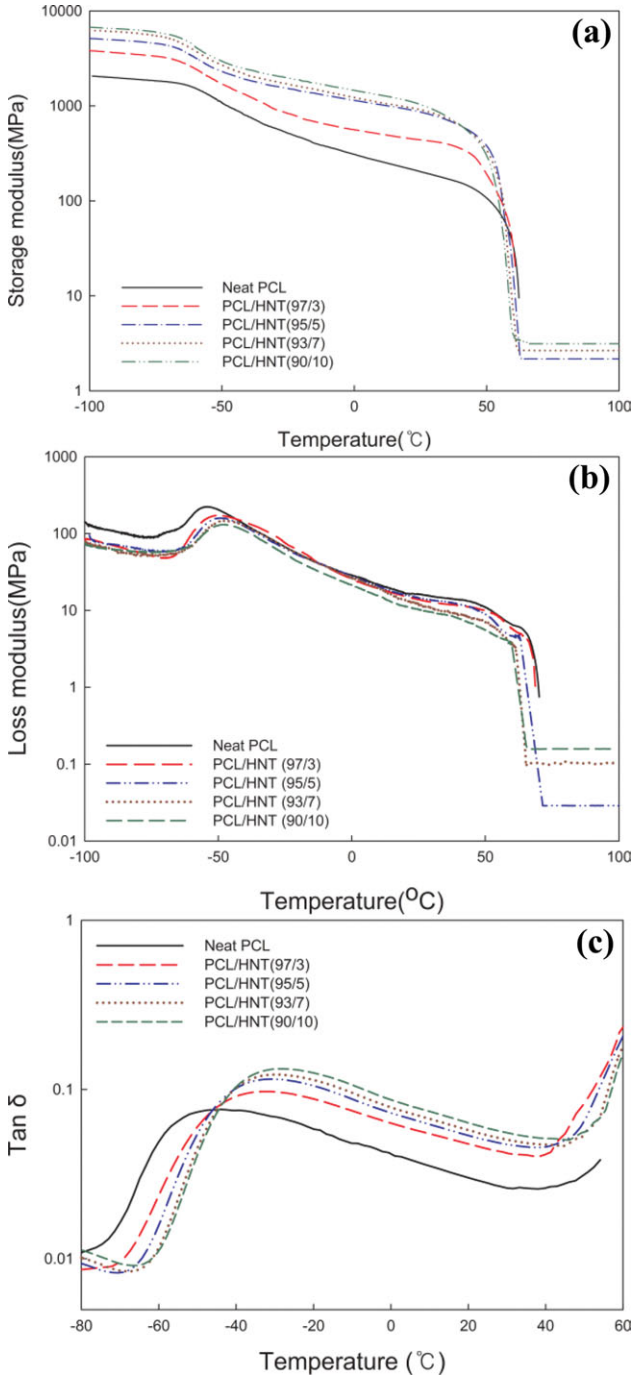

Figure 7. Variations in (a) storage modulus, (b) loss modulus, and (c) tan δ with temperature for neat PCL and PCL/HNT nanocomposites. [Color figure can be viewed in the online issue, which is available at wileyonlinelibrary.com.]

Nanostructured Morphology

TEM photographs of ultrathin sections of compression-molded PCL/HNT nanocomposites are illustrated in Figure 5. It is apparent that the individually separated HNTs, about 50–70 nm

Table II. Dynamic Mechanical Properties of PCL/HNT Nanocomposites

Samples	T_g from tan δ peak (°C)	T_g from E'' peak (°C)	E' at -25°C (MPa)	E' at 25°C (MPa)	E' at 70°C (MPa)	Tan δ at T_g (°C)
Neat PCL	-44.3 ± 0.1	-54.15 ± 0.1	520 ± 5	202 ± 3	0.00	0.076 ± 0.004
PCL/HNT						
97/3	-35.1 ± 0.1	-50.57 ± 0.1	861 ± 2	439 ± 2	0.00	0.096 ± 0.005
95/5	-32.9 ± 0.1	-49.21 ± 0.1	1506 ± 4	801 ± 2	2.16 ± 0.03	0.115 ± 0.003
93/7	-32.2 ± 0.1	-48.71 ± 0.1	1711 ± 1	911 ± 5	2.65 ± 0.05	0.122 ± 0.004
90/10	-31.4 ± 0.1	-48.30 ± 0.1	1979 ± 3	1034 ± 2	3.13 ± 0.04	0.132 ± 0.002

in diameter, are uniformly dispersed in the matrix polymer and some aggregated HNTs coexist in the samples with higher loadings of HNTs. The TEM photographs also show that the HNTs are randomly oriented. It should be stressed that the integrity of the nanotubes is destroyed when the nanocomposite samples are cut using an ultra-microtome. The nanoscaled dispersion of HNTs indicates that there is a certain extent of compatibility between the surface of the HNT and PCL. The driving force for homogeneous dispersion of HNT within the PCL matrix is due to the high shear force at the time of melt mixing and strong interfacial interactions between PCL and HNT because of great affinity of PCL for HNTs. Similar results were also reported for nanocomposites of unmodified HNTs with nylon 6 and nylon 12 prepared by melt blending, where HNTs were homogeneously dispersed in the matrix polymer.[12,13]

Thermal Properties

Thermal characterization of the PCL/HNT nanocomposites was carried out using DSC measurements. The DSC thermograms of the samples in the cooling process after the melt and in the re-melting process are shown in Figure 6(a, b), respectively. The melting temperature (T_m), heat of fusion (ΔH_m), and associated degree of crystallinity (χ_c) as well as the non-isothermal crystallization peak temperature (T_c) obtained from the DSC thermograms are summarized in Table I. The degree of crystallinity of the nanocomposites was calculated using the heat of fusion per gram of PCL determined from DSC measurements and the heat of fusion corresponding to 100% crystalline PCL (136 J/g).[31] It is shown in Table I that the values of T_m and the χ_c are reduced in case of the nanocomposites as compared to the neat PCL. This is due to the decrease in molecular mobility of the PCL chains in the nanocomposites that causes a reduction in the PCL crystal size and imperfections of the crystals. Similar behavior was also observed for PCL/clay nanocomposites.[20]

In the cooling process, the nanocomposites showed higher crystallization peak temperatures than neat PCL, and the crystallization temperature increased with increasing HNT content in the nanocomposites. This result indicates that HNTs act as nucleating agents and causes the crystallization rate to increase, i.e., the formation of the nuclei occurred earlier during cooling after the melt. The same effect has been reported for PCL nanocomposites based on clay and CNTs[21,24] and nylon 6/HNT nanocomposites.[12]

Dynamic Mechanical Properties

Figure 7(a) shows the variation in the storage modulus (E') with temperature for neat PCL and PCL/HNT nanocomposites, respectively, and the results are summarized in Table II. As shown, the storage moduli for the nanocomposites are higher than those of neat PCL over the whole temperature range examined here, and the modulus increased with increasing HNT content, implying that the HNT nanoparticles acted as reinforcing fillers. It is also notable in Figure 7(a) that the storage modulus for neat PCL continued to decrease with temperature and the material flows like a viscous liquid when the temperature is greater than T_m, whereas PCL/HNT nanocomposites showed a persistent rubbery plateau above T_m when the HNT content was above 5 wt %. The presence of a persistent rubbery plateau in the PCL/HNT nanocomposites indicates that the nanocomposites formed a physically crosslinked structure due to the strong interfacial interactions polymer matrix and HNT. The high intrinsic stiffness of HNT resulting from its highly dimensionally stable tubular nanostructure also have adequate amount of contribution to the occurrence of rubbery plateau. In the rubbery plateau region, the storage modulus values, which are directly related to the degree of crosslinking of the sample, increased with increasing HNT content in the nanocomposites.

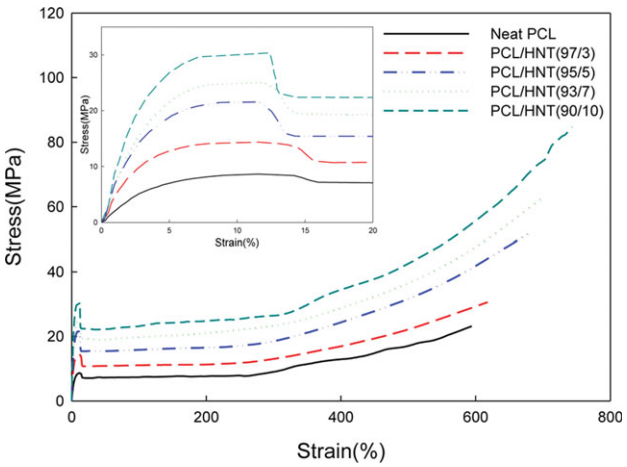

Figure 8. Tensile stress–strain curves of neat PCL and PCL/HNT nanocomposites. [Color figure can be viewed in the online issue, which is available at wileyonlinelibrary.com.]

Table III. Tensile Properties of PCL/HNT Nanocomposites

Samples	E' (MPa)	σ_y (MPa)	σ_b (MPa)	ε_y (%)	ε_b (%)
Neat PCL	206 ± 7	8.7 ± 0.1	23.1 ± 0.5	11.5 ± 0.1	590 ± 30
PCL/HNT					
97/3	263 ± 12	14.7 ± 0.4	30.6 ± 0.5	11.6 ± 0.1	617 ± 35
95/5	382 ± 27	21.6 ± 0.4	52.3 ± 0.6	11.6 ± 0.1	682 ± 38
93/7	675 ± 32	25.0 ± 0.4	63.4 ± 0.6	11.7 ± 0.1	703 ± 35
90/10	919 ± 38	30.3 ± 0.5	84.7 ± 0.6	12.4 ± 0.1	743 ± 36

E is Young's modulus, σ_y is the yield stress, σ_b is the tensile strength, ε_y is the strain at which yielding occurs, and ε_b is elongation at break.

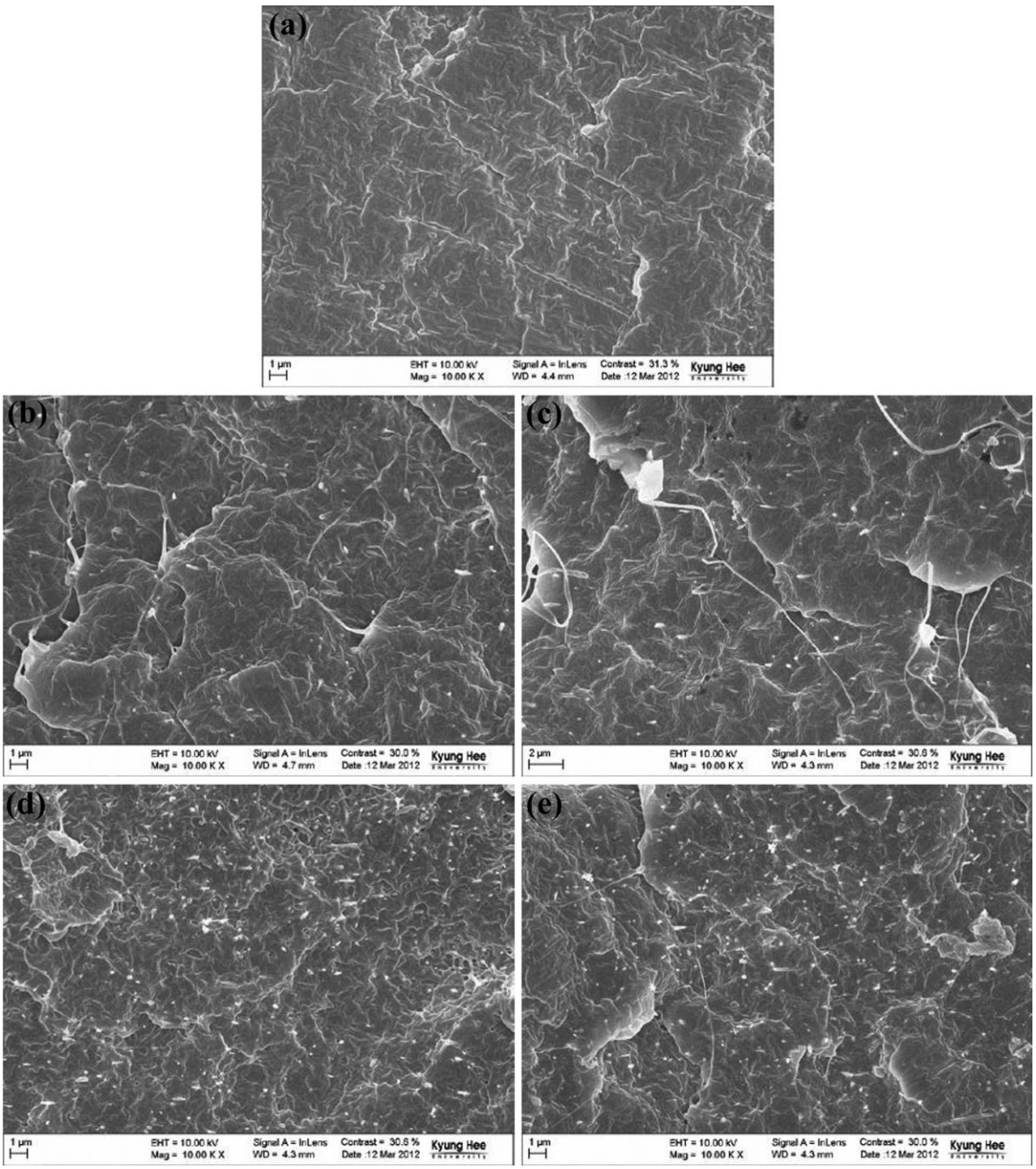

Figure 9. SEM cryo-fractured microphotographs of (a) neat PCL and PCL/HNT nanocomposites: (b) 97/3, (c) 95/5, (d) 93/7, and (e) 90/10.

Applied Polymer SCIENCE

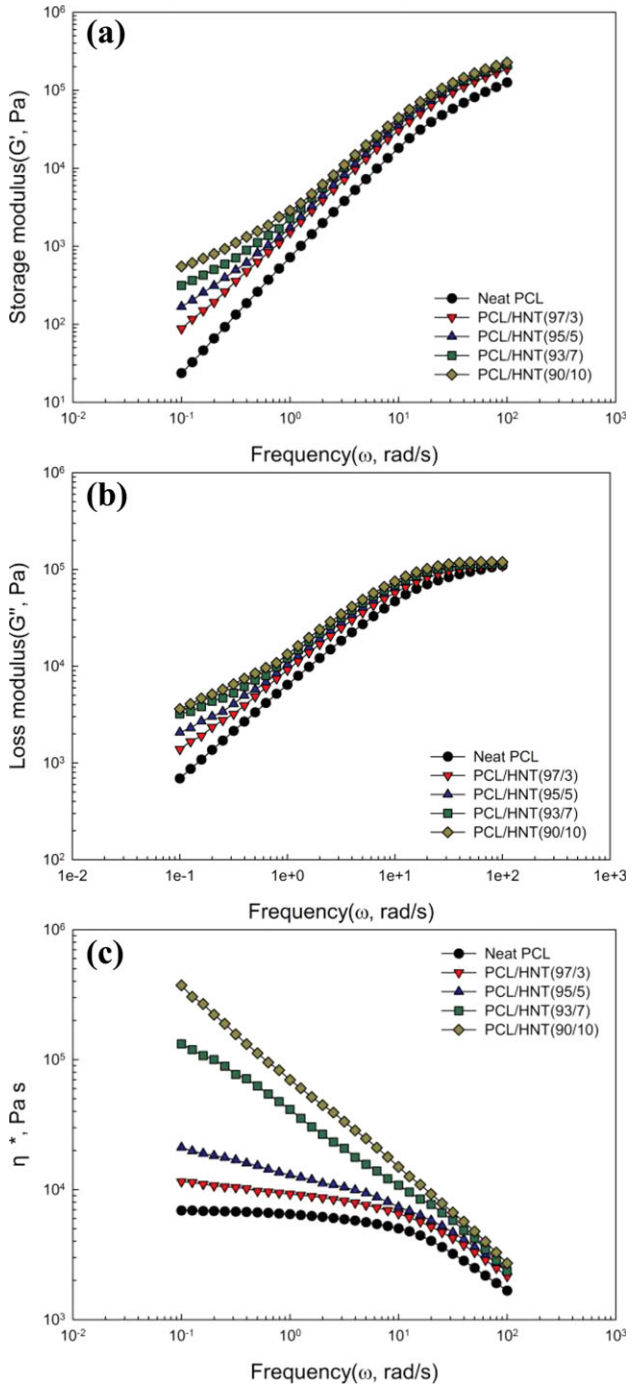

Figure 10. Frequency dependence of the (a) storage modulus (G'), (b) loss modulus (G''), and (c) complex viscosity (η^*) at 100°C for both neat PCL and PCL/HNT nanocomposites. [Color figure can be viewed in the online issue, which is available at wileyonlinelibrary.com.]

The dependence of loss modulus (E'') on temperature is shown in Figure 7(b). It is observed that the values of E'' reduced in the HNT-filled system as compared to the pristine counter parts, which is due to the reduction of viscous component of the polymer matrix by the presence of rigid HNT. It is observed from Table II that the broad peak centered at around –54°C is attributed to T_g of the PCL matrix, which is increased by 5°C with addition of HNT nanofillers because the dimensionally stable HNTs restricted the segmental mobility of the molecular chains. It is informed that the HNTs successfully impart reinforcing effect on the PCL matrix. At higher temperature region, the neat PCL did not sustain but HNT-filled systems exhibit a plateau resulted from the development of physical crosslinking network throughout the PCL matrix.

It is evident from Figure 7(c) and Table II that the glass transition temperature (T_g) of the PCL/HNT nanocomposites, determined from the position of the peak maximum in the tan δ, was higher than that of neat PCL, and the values were shifted toward higher values with increasing HNT content in the nanocomposites. This indicates that the HNTs imposed constraints on the polymer chains of the PCL and decreased the molecular mobility of amorphous PCL chains in the nanocomposites. This is also caused due to the high strength and stiffness of rigid HNTs along with its evenly dispersion throughout PCL matrix. The tan δ value is not reduced sharply and not returned back to minimum after reaching a maximum. The peak was broadened at the higher temperature region by the addition of HNT into PCL matrix. It is concluded that the polymer segments with close proximity to HNT has comparatively less mobility than that of the segments away from the HNT, as a consequence the T_g of the system significantly increased.[26] The tan δ value abruptly increases at temperature above 40°C, which may be due to the softening of the polymer result in more viscous component to elastic component. The area under the tan δ peak increases with increase in HNT loading, which indicates the damping characteristic of the PCL nanocomposites that significantly increased by the incorporation of HNTs.

Tensile Properties

The stress–strain curves of neat PCL and PCL/HNT nanocomposites are shown in Figure 8, and the results are summarized in Table III. The tensile strength and modulus of the PCL matrix is substantially enhanced by the inclusion of HNT, which is attributed to the good compatibility of the HNTs with PCL system as well as uniform dispersion of HNTs. Neat PCL exhibits typically ductile behavior, undergoing a large deformation (about 600% strain) with yielding followed by a deformation under constant stress and subsequent strain hardening. PCL/HNT nanocomposites exhibited similar ductile deformation along with a higher tensile modulus, yield strength, and elongation at break compared to neat PCL. The increase in elongation at break for HNT-filled PCL matrix than that of pristine counterpart is a unusual case but this type of behavior is observed for organically modified montmorillonite-based PCL nanocomposites.[32] This is due to the strong strain hardening of the PCL matrix imparted by the rigid HNTs. Similar observations were reported for nanocomposites based on nylon 6 with as-received HNTs[11] and hydroxyapatite nanocrystals based PCL nanocomposites.[33]

Cryo-Fractured Morphology

The cryo-fractured morphology of the neat PCL and PCL/HNT nanocomposites were analyzed by using SEM as shown in Figure 9. It is observed that the surface roughness of the fractured surface increases with increase in wt % of HNT nanotube

Table IV. Terminal Region Slopes and η^* of Neat PCL and PCL/HNT Nanocomposites

Samples	Slope of G'	Slope of G''	η^* at 1 rad/s (Pa s)
Neat PCL	1.54 ± 0.03	1.00 ± 0.02	$6.46 \pm 0.05 \times 10^2$
PCL/HNT			
97/3	1.23 ± 0.02	0.81 ± 0.01	$9.26 \pm 0.03 \times 10^2$
95/5	1.01 ± 0.02	0.69 ± 0.01	$1.30 \pm 0.02 \times 10^3$
93/7	0.84 ± 0.01	0.56 ± 0.01	$3.53 \pm 0.04 \times 10^3$
90/10	0.72 ± 0.01	0.54 ± 0.01	$6.03 \pm 0.04 \times 10^3$

loading. The presence of HNT nanotube dramatically alters the fracture propagation direction that causes excess dissipation of the external energy, as a consequence the tensile strength and modulus of the PCL/HNT nanocomposites significantly increased as compared to the pristine PCL matrix. It is evident from the microphotographs that the HNT nanotubes are homogeneously dispersed within the PCL matrix without any HNT clusters even if at 10 wt % HNT loading. The individual nanotube is not pulled out of the matrix rather it was ruptured into two parts and the absence of any parting lines, voids, and cavities in the micrographs imply that there is development of very good wetting and adhesion bonding among PCL and HNT.

Rheological Properties

The melt rheological behavior of the PCL/HNT nanocomposites was studied in order to get an idea of the microstructure in the melted state. Melt rheological behavior is also important from a processing point of view. The elastic modulus (G') and the loss modulus (G'') of neat PCL and PCL/HNT nanocomposites are shown in Figure 10(a, b), respectively. It is apparent in the figures that the G' and G'' of the nanocomposites are higher than those of neat PCL, which is attributed to the good interphase attraction between PCL and HNT, and homogeneous dispersion of HNT within PCL matrix. The increase in the modulus is prominent in the lower frequency range, and the difference decreases at higher frequencies. Thus, at higher frequencies, the rheological behavior of the nanocomposites is dominated by the polymer rather than the nanofiller. The storage modulus and loss modulus increased with increasing frequency. This is due to the fact that, at low frequencies, there is enough time to unravel the entanglements so that a large degree of relaxation can occur, which results in a lower loss and storage modulus. When a polymer sample is deformed at a high frequency, the entanglements do not have sufficient time to relax and, therefore, the modulus increases. The slope of the both G' and G'' curves in the near terminal region, i.e., below 5 rad/s frequency were calculated and tabulated in Table IV. It was observed that the slopes of G' and G'' of the PCL/HNT nanocomposites are smaller than those of neat PCL. The higher G' and smaller terminal slope of the nanocomposites over their unfilled counterpart indicates the formation of a three-dimensional superstructure in the nanocomposites. These results are in good agreement with the rheological behavior of nylon 12/HNT nanocomposites[13] and PCL/clay nanocomposites.[20] The slope of G'' versus frequency curve also decreases with HNT loading at low frequency region due to the formation of network structures between PCL and HNT.

The change in complex viscosity (η^*) of the neat PCL and PCL/HNT nanocomposites is shown in Figure 10(c). At lower frequency region, the pristine PCL shows a frequency independent horizontal viscosity zone corresponding to the Newtonian flow followed by reduction of η^* with increase in frequency called pseudo-plastic behavior. This effect is continued up to 5 wt % HNT loading but after that it is completely diminished due to the strong shear thinning behavior resulted from the aggregation of HNTs within the PCL matrix.[34] PCL/HNT nanocomposites show more pronounced shear thinning behavior as compared to neat PCL. This shear thinning behavior indicates good processability of the nanocomposite. The values of η^* of the nanocomposites were higher than that of its unfilled counterpart throughout the scanned frequency range. It is evident in Table IV that the complex viscosity of the nanocomposites containing 10 wt % of HNTs is about 10-fold higher than that of neat PCL at 1 rad/s. Such enhanced viscosity of the polymer nanocomposites is attributed to the flow restriction of polymer chains in the molten state by the nanoparticles.

CONCLUSIONS

This study demonstrated that pristine, unmodified HNTs can be dispersed on the nanometer scale in a PCL matrix by a melt-mixing process. The contact angle measurement showed that contact angle of the PCL/HNT nanocomposites decreased and wetting energy increased with the addition of HNT nanofillers that resulted good adhesion bonding among them. The reduction in the binding energy of the characteristic bonds with HNT loading further confirms the formation of interfacial interactions between PCL and HNT. The presence of the nanoparticles induced a decrease in both T_m and the degree of crystallinity of the PCL, and the HNTs in the nanocomposites acted as nucleating agents during non-isothermal crystallization. The value of E' of the PCL matrix was significantly increased with increase in HNT content. The tan δ peak temperature termed as dynamic T_g of the PCL matrix shifted to the higher temperature region by the incorporation of HNT. A small amount of HNTs led to substantial increases in tensile modulus and strength without a loss in ductility of the PCL. The cryo-fractured morphology revealed that the HNTs were uniformly dispersed throughout the PCL matrix and the roughness of the fracture surface was also increased significantly that controls the micro-crack propagation. The melt rheological study revealed that the PCL/HNT nanocomposites exhibited a more pronounced solid-like and stronger shear thinning behavior as compared to neat PCL, which were more prominent at higher HNT content.

ACKNOWLEDGMENT

This study was supported by the research fund SRC/ERC program of MEST (Grant number: R11-2005-056-04004-0).

REFERENCES

1. Giannelis, E. P. *Adv. Mater.* **1996,** *8*, 29.
2. Moniruzzaman, M.; Winey, K. L. *Macromolecules* **2006,** *39*, 5194.
3. Paul, D. R.; Robeson, L. M. *Polymer* **2008,** *49*, 3187.

4. Zou, H.; Wu, S.; Shen, J. *Chem. Rev.* **2008,** *108*, 3893.
5. Shi, Y.-F.; Tian, Z.; Zhang, Y.; Shen, H.-B.; Jia, N.-Q. *Nanoscale Res. Lett.* **2011,** *6*, 608.
6. Joussein, E.; Petit, S.; Churchman, J.; Theng, B.; Righi, D.; Delvaux, B. *Clay Miner.* **2005,** *40*, 383.
7. Lvov, Y. M.; Shchukin, D. G.; Mohwald, H.; Price, R. R. *ACS Nano* **2008,** *2*, 814.
8. Du, M.; Guo, B.; Jia, D. *Polym. Int.* **2010,** *59*, 574.
9. Zia, Z.; Luo, Y.; Guo, B.; Yang, B.; Du, M.; Jia, D. *Polym. Plast. Technol. Eng.* **2009,** *48*, 607.
10. Du, M.; Guo, B.; Jia, D. *Eur. Polym. J.* **2006,** *42*, 1362.
11. Marney, D. C. O.; Russell, L. J.; Wu, D. Y.; Nguyen, T.; Cramm, D.; Rigopoulos, N.; Wright, N.; Greaves, M. *Polym. Degrad. Stab.* **2008,** 93, 1971.
12. Hedicke-Hochstotter, K.; Lim, G. T.; Altstadt, V. *Compos. Sci. Technol.* **2009,** *69*, 330.
13. Lecouvet, B.; Gutierrez, J. G.; Sclavons, M.; Bailly, C. *Polym. Degrad. Stab.* **2011,** *96*, 226.
14. Deng, S.; Zhang, J.; Ye, L.; Wu, J. *Polymer* **2008,** *49*, 5119.
15. Rooj, S.; Das, A.; Thakur, V.; Mahaling, R. N.; Bhowmick, A. K.; Heinrich, G. *Mater. Des.* **2010,** *31*, 2151.
16. Ismail, H.; Pasbakhsh, P.; Ahmad Fauzi, M. N.; Abu Kakar, A. *Polym. Test.* **2008,** *27*, 841.
17. Zhixin, J.; Yuanfang, L.; Shuyan, Y.; Mingliang, D.; Baochun, G.; Demin, J. *J. Nanosci. Nanotechnol.* **2011,** *11*, 10958.
18. Wang, Y.; Rodriguez-Perez, M. A.; Reis, R. L.; Mano, J. F. *Macromol. Mater. Eng.* **2005,** *290*, 792.
19. Messersmith, P. B.; Giannelis, E. P. *Chem. Mater.* **1993,** *5*, 1064.
20. Lepoittevin, B.; Devalckenaere, M.; Pantoustier, N.; Alexandre, M.; Kubies, D.; Calberg, C.; Jerome, R.; Dubois, P. *Polymer* **2002,** *43*, 4017.
21. Gain, O.; Espuche, E.; Pollet, E.; Alexandre, M.; Dubois, P. H. *J. Polym. Sci. Part B: Polym. Phys.* **2005,** *43*, 205.
22. Luduena, L. N.; Alvarez, V. A.; Vazquez, A. *Mater. Sci. Eng. A* **2007,** 460–461, *121*.
23. Liu, Q.; Peng, Z.; Chen, D. *Polym. Eng. Sci.* **2007,** *47*, 460.
24. Avella, M.; Bondioli, F.; Cannillo, V.; Pace, E. D.; Errico, M. E.; Ferrari, A. M.; Focher, B.; Malinconico, M. *Compos. Sci. Technol.* **2006,** *66*, 886.
25. Chen, E. C.; Wu, T. M. *Polym. Degrad. Stab.* **2007,** *92*, 1009.
26. Saeed, K.; Park, S. Y. *J. Appl. Polym. Sci.* **2007,** *104*, 1957.
27. TA Instruments. Thermal Solutions: Measurement of the Glass Transition Temperature Using Dynamic Mechanical Analysis. http://www.tainstruments.com/pdf/literature/TS64.pdf.
28. ASTMD 412-06a (2006), Standard Test Methods for Vulcanized Rubber and Thermoplastic Elastomers-Tension. ASTM International, Pennsylvania, USA.
29. Thomas, S. P.; Thomas, S.; Abraham, R.; Bandyopadhyay, S. *Express Polym. Lett.* **2008,** *2*, 528.
30. Du, M.; Guo, B.; Lei, Y.; Liu, M.; Jia, D. *Polymer* **2008,** *49*, 4871.
31. Avella, M.; Errico, M. E.; Laurienzo, P.; Martuscelli, E.; Raimo, M.; Rimedio, R. *Polymer* **2000,** *41*, 3875.
32. Neppalli, R.; Causin, V.; Marega, C.; Saini, R.; Mba, M.; Marigo, A. *Polym. Eng. Sci.* **2011,** *51*, 1489.
33. Hao, J.; Yuan, M.; Deng, X. *J. Appl. Polym. Sci.* **2002,** *86*, 676.
34. Liu, Q.; Chen, D. *Eur. Polym. J.* **2008,** *44*, 2046.